Microelectronic Engineering 210 (2019) 14–18

Contents lists available at ScienceDirect

Microelectronic Engineering

journal homepage: www.elsevier.com/locate/mee

Research paper

Development of silicon microneedle arrays with spontaneously generated micro-cavity ring for transdermal drug delivery

Alakananda Das[a], Chirantan Singha[b], Anirban Bhattacharyya[a,*]

[a] Institute of Radio Physics and Electronics, University of Calcutta, Kolkata 700009, India
[b] Centre for Research in Nanoscience and Nanotechnology, University of Calcutta, Kolkata 700106, India

ARTICLE INFO

Keywords:
Silicon
Micro-machining
Crystallographic etch
Drug delivery
Scanning electron microscopy
Microfluidics

ABSTRACT

Transdermal drug delivery techniques based on microneedle arrays can painlessly administer controlled amount of drugs through penetration of the epidermis. Solid microneedles arrays can be employed in this process after coating the tip with the liquid agent before insertion. In this work, we report a low cost technique for the formation of pyramidal microneedle arrays based on crystalline silicon. A combination of crystallographic etching, thermal oxidation and subsequent HNA treatment was employed. Optimization of the process parameters led to the generation of pyramidal microneedle arrays where the tip diameter can be reduced without loss of overall structural robustness. Micro-cavities with size 4–10 μm in diameter can be reproducibly generated in a ring surrounding the tip, while maintaining an otherwise smooth microneedle facet wall. Optical fluorescence imaging indicates that fluids can be exclusively trapped in these microcavities, with implications in transdermal drug delivery.

1. Introduction

There is a major drive towards the development of low cost, biocompatible, structurally robust microneedles for dermal and transdermal drug delivery [1]. These structures, which have heights in the range 300 μm to 1 mm, have tip diameters around 2–25 μm [2,3], and can be used to pierce the upper layer of the skin to withdraw body fluids or to inject drugs in a painless manner. Furthermore, microneedles can be integrated into "lab-on-a-chip" (LOC) systems where the testing of the fluids can be carried out at the chip level, and the results automatically communicated to medical professionals [4]. Microneedles can be either hollow or solid, and for each class there are different approaches of drug delivery. For hollow microneedles a drug in solution is actively or passively delivered through the bore of the microneedles [5]. There are several approaches for solid microneedles for transdermal drug delivery. Micro-pores may be generated in the skin using microneedle arrays followed by application of a patch, thereby allowing the drug in the patch to diffuse through the skin [6]. Alternatively, the drug can be contained in the needle itself, and released after puncture, which requires the use of dissolvable or porous microneedles [7]. Finally, solid microneedles coated with a specific drug may be pierced through the skin, thereby releasing the chemicals through hydration of the coating.

Various materials have been used in the fabrication of solid and hollow microneedle structures, including polymers [8–10], metals [11] as well as semiconductors [12]. Silicon micromachining is an important tool in the development of such structures, using either reactive ion etching [13] or the wet chemical etching process. Several groups have also fabricated solid microneedles with porous tip [14] where drugs can be stored during the delivery process. While porous silicon is a non-toxic and biocompatible material [15] that has been produced with a large variety of pore sizes [16–18], porous silicon microneedles may easily break and stay inside the skin upon piercing. Nevertheless, the general concept of inclusion of pores or micro-cavities into microneedle tips without loss of sharpness is a useful route to transdermal drug delivery. Control over the micro-cavity dimensions while maintaining a low cost, scalable process is critical for this application. In this paper we investigate the development of such silicon microneedles with spontaneously formed micro cavities using a combination of isotropic [19] and anisotropic wet chemical etch process.

2. Experimental methods

500 μm thick silicon substrates with (100) orientation were employed for this work. They were doped with boron (resistivity of 1–10 Ω-cm) and were procured pre-coated with 2 μm thick thermal SiO_2 layers on both sides. Prior to microfabrication, the wafers were degreased using trichloroethylene, acetone, isopropyl alcohol and de-

* Corresponding author.
E-mail address: anirban.rpe@caluniv.ac.in (A. Bhattacharyya).

https://doi.org/10.1016/j.mee.2019.03.019
Received 24 September 2018; Received in revised form 19 March 2019; Accepted 22 March 2019
Available online 23 March 2019

ionized water. Photolithography processes were carried on a Suss MicroTec MA6-BA6 Mask Aligner/Exposure system using S1813photoresist and MF26A developer (Shipley), employing standard recipes.

Etching of silicon dioxide (SiO_2) was carried out using buffer oxide etch (BOE) process at room temperature. A KOH bath was employed for the crystallographic etching of silicon. The samples were immersed in KOH solution (Molarity = 3.28 mol/cc) at 80 °C and the solution was stirred continuously. The surface of the wafer was kept at an angle of 45 degree facing downwards during the entire process. The selectivity of etch of (100) planes over (111) planes was further enhanced by introduction of isopropyl alcohol at 1:5 ratio in the KOH solution. This process was monitored in real time using a LEICA WILD 40 macroscope. Oxidation was carried out using a tube furnace equipped with a water bubbler. An HNA (4:7:11) solution was used for isotropic etch with or without stirring. The etched structures were investigated by scanning electron microscopy (SEM) using a Zeiss EVO18 system. Optical and fluorescence imaging was carried out using a Leica DM2700M.

3. Results and discussions

3.1. Single step process: formation of pyramidal structures

Fig. 1(a)–(d) indicates the fabrication process steps employed for the generation of micropyramidal arrays by wet chemical etching process. Arrays of square features with sides ranging from 80 × 80 μm to 140 × 140 μm with various spacing were formed on the SiO_2 surface. Care was taken to align the edge of the box like structures along the

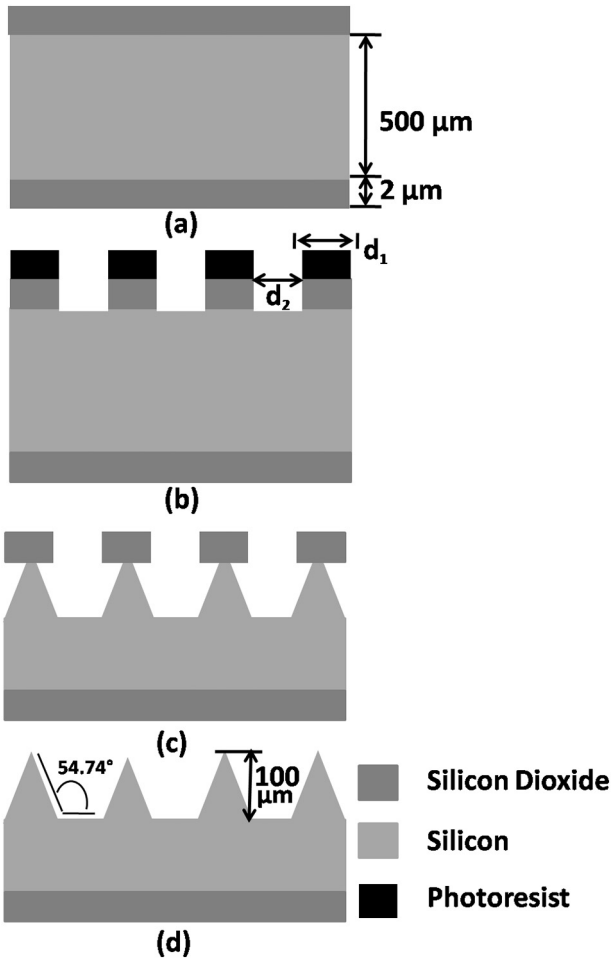

Fig. 1. Fabrication steps of Silicon micro-pyramidal array using crystallographic etch.

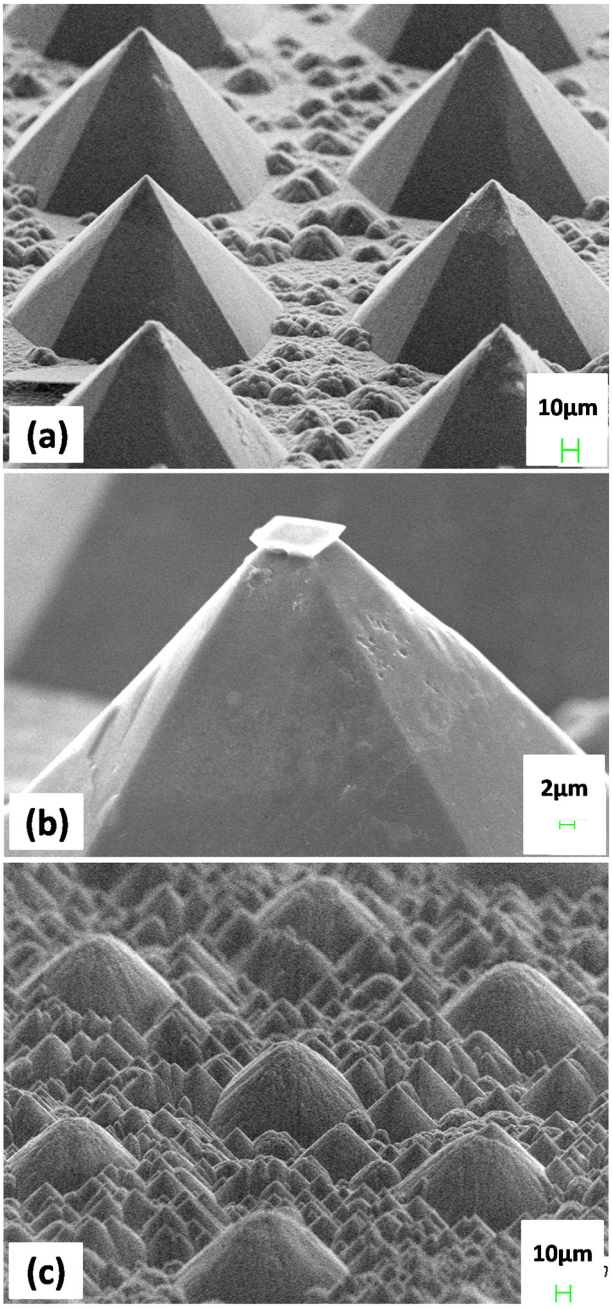

Fig. 2. SEM images showing micropyramids with (a) sharp tips, (b) incomplete SiO_2 undercut and (c) rounded tops due to over-etch.

[100] direction of the wafer in order to assist subsequent crystallographic etch. The SiO_2 layer was then selectively etched using a buffer oxide etch (BOE) solution at room temperature, generating an etch rate of 0.83 nm/s (Fig. 1b). After removing the photoresist, crystallographic etch of the silicon wafer surface was carried out as shown schematically in Fig. 1(c).

The scanning electron micrograph of the etched silicon surface is shown in Fig. 2. An etch rate of up to 8.89 nm/s was achieved, under optimized conditions. Square SiO_2 regions formed after the step (b) as described in Fig. 1 functions here as the mask for the crystallographic wet chemical etching.

However, we observed that it is very difficult to terminate the process at the appropriate end-point, that is when the undercutting process is just completed. Under optimal conditions, uniform, well

oriented arrays of micropyramids can be formed, each with clearly defined facets on an octahedral base and a sharp tip. This is shown in Fig. 2(a), where the SEM images of such structures are presented. However, small changes in the process conditions, such as local solution strength, temperature as well as sample geometry can cause the process to be stopped prematurely, where the top surface is still covered with the SiO_2 layer, as in Fig. 2(b). Here the SEM microscopy image shows the top SiO_2 layer, which has dimensions of several μm, and is therefore not easy to image using low magnification optical microscopy. This can be removed by a BOE etch process, revealing a truncated pyramidal structure with a top plateau. This plateau again can vary in width depending on the non-uniformities described previously. In the other extreme, if the sample is kept in a KOH bath after the top SiO_2 mask layer has been removed, it may lead to a subsequent etching of the tip, thereby rounding it, as shown in Fig. 2(c). While truncated pyramids have many applications, this rounding of the top surface is clearly undesirable, but difficult to avoid, especially for large wafers.

3.2. Two-step process: narrowing of the tip

In order to increase the stability of the fabrication process, a two step approach was taken to separate out the process steps of (a) formation of truncated top micro-pyramid, and (b) wet chemical etch to narrow the tip. The last process step is based on the dependence of thermal oxidation of silicon on surface morphology, that is sharp edges are oxidized faster than flat surfaces [20]. In the two step process, the initial crystallographic etch process as described previously was terminated at a stage where there was still a small flat plateau on the top.

Subsequently, wet oxidation was performed on these micro pyramidal structures in a tube furnace at 950 °C for 10 h. The thickness of the oxide layer grown under similar conditions on a flat (unetched) silicon wafer was measured by spectroscopic ellipsometry to be about approximately 870 nm. However, as shown schematically in Fig. 3, it is expected that the flat sidewalls and top plateaus of the silicon micro pyramids will be oxidized slower than the corner of the plateaus. A subsequent buffer oxide etch removes the SiO_2 from all regions, and leaves the tip narrower than it was originally.

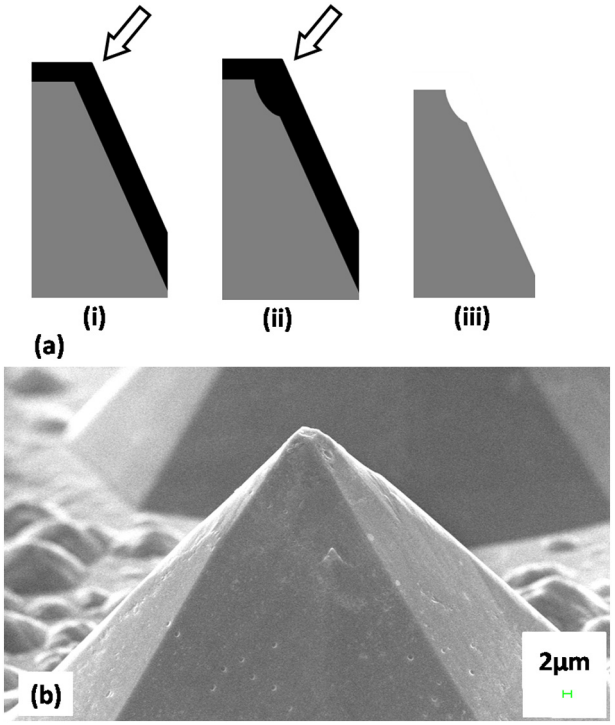

Fig. 3. (a) Schematic showing the sharpening of the micropyramids employing oxidation and subsequent etching steps, (b) SEM image of the resultant structure.

This can be observed clearly in the SEM image shown in Fig. 3(b) of an originally truncated pyramidal structure that has been oxidized and subsequently exposed to BOE process. In this process, the top flat plateau has been reduced to a square of less than 2 μm in dimension, which is acceptable for most biomedical micro-needle applications. This process eliminates the need for precise process termination that was necessary in the crystallographic etch process. The oxidation step can be modified in time and temperature in order to account for a larger or a smaller top pyramidal plateau. Several groups have attempted to develop sharp microneedle structures by the isotropic etching process, generating thereby tip diameters that are significantly narrower. However that process requires a silicon nitride mask, which requires a CVD process and is significantly more complex than the thermal oxidation process required for this work.

3.3. Three step process: formation of microcavities

Finally, we have investigated the effect of HNA etch process on the truncated pyramidal structures fabricated by anisotropic KOH etching. Pyramidal structures were formed by the process described in Section 3.1, and thermally oxidized as previously described in Section 3.2. Subsequently they were dipped in a BOE bath at room temperature for 40 min. During this process, all the SiO_2 including the top cap layer was removed.

A bath of HF: HNO3: Acetic acid of 4:7:11 was kept at room temperature, and the samples were immersed at 45 degree angle, facing downwards for 5 min. Two sets of samples were prepared, one where the solution was stirred at 120 rpm, and for the other the solution was kept stagnant. The structures were then rinsed, dried and examined by scanning electron microscopy.

The SEM image of array structures after the HNA process where the solution was stirred is shown in Fig. 4(a). As can be seen, the arrays have become significantly narrower without any rounding off of the edges. The tip geometry was changed from octagonal to square and the diameter was reduced form 25–30 μm to 10 μm. The sidewalls have also evolved from interlinked (311) and (111) planes observed previously, to a more regular structure bound by only the (111) planes.

An interesting effect was observed when the solution was not stirred during the HNA etch process. While smooth sidewalls were observed for samples where the solution was stirred, for these samples the sidewalls were found to contain a number of micro-cavity structures. For long HNA etch times, such microcavities are produced on the pyramidal sidewalls (Fig. 4(b)), and are about 20–30 μm in diameter. Their density has also been found to be dependent on other parameters, such as array geometries.

Under optimized conditions, specifically for short HNA etch times, carried out without stirring the solution, we have obtained microneedles where the tip-edge was completely decorated with a large number of micro-cavity structures, each varying from 4 to 10 μm in diameter. Thus, using a simple combination of crystallographic KOH etch, followed by thermal oxidation and finally HNA etching process, we have obtained microneedle arrays with integrated micro-cavity structures that can be used for the storage of agents during drug delivery through the skin. Aside from the simplicity and low cost process, these structures are also very robust, as the sidewalls are (111) crystal planes. The tip is also not completely porous, and is not significantly weakened by the presence of the micro-cavities thereby reducing the possibility of breakage during insertion.

The formation of these microcavities can be linked to two possible phenomena. During the thermal oxidation of the microneedle structure, while the flat surfaces are oxidized uniformly, for sharper edges like those surrounding the top facet the oxidation rate can vary widely. This can lead to formation of LOCOS type structures, which etch away during the later processes. Another reason for these cavities can be that

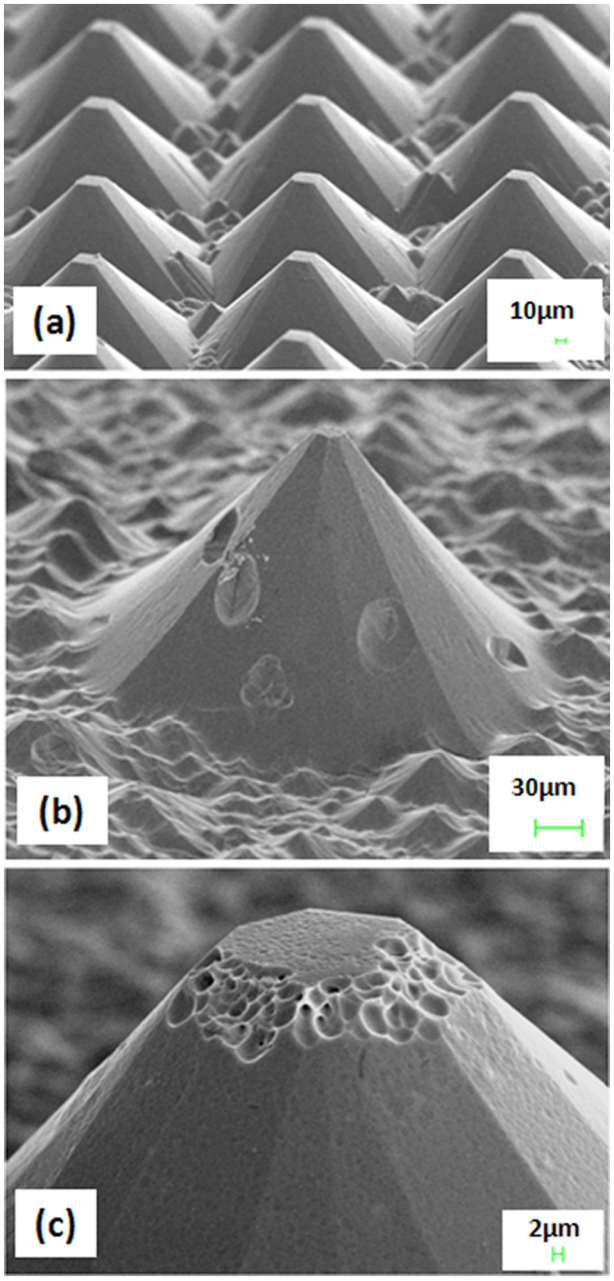

Fig. 4. SEM image showing (a) the micro pyramidal array with significantly narrower tip (b) the micropyramids with microcavities on the pyramidal sidewalls and (c) microcavity ring surrounding the tip.

there are small chemical composition fluctuations in the HNA solution, specially around structures like the tip of the pyramids, where the localized etch rate can be quite high due to the presence of defects generated from the earlier KOH etch process at the meeting point of various facets. These localized defects then are removed selectively, thereby generating microcavities as the material around each defect is removed faster than the general silicon layers. Our observation is that if there is no stirring of the liquid during the HNA step, for short duration, the cavities are formed exclusively on the top edge, and the microcavities are formed randomly all over the sides of the pyramids if the etching process is continued for a long period. Therefore, this process can be optimized to obtain any degree of surface porosity as desired.

In order to verify that the series of microcavities generated at the edge of the top plateau of the microneedle are appropriate for storage of liquid droplets, optical microscopy was carried out using a LEICA

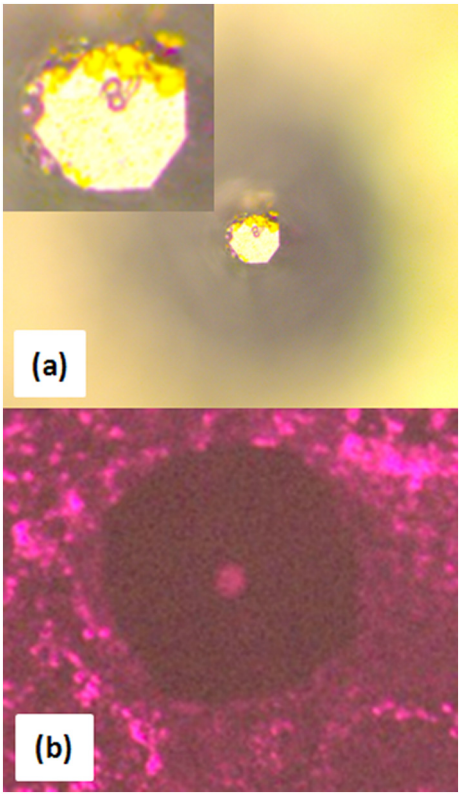

Fig. 5. Visible light microscopy image (a) and Fluorescence image (b) of a microneedle with microcavities filled with Rhodamine B dye. Inset in (a) shows a magnified view of the microneedle tip.

DM2700 system. The microneedles were coated with Rhodamine B dye using a standard applicator, and illuminated with either visible light, or with a hand-held UV source with excitation at 365 nm.

A visible light microscopy image is presented in Fig. 5(a), showing the entire micro-needle structure with the top plateau in focus. A higher magnification image shown in the inset indicates that the top plateau is octagonal and about 30 µm in diameter. The Rhodamine B dye can be observed in the form of droplets about 6–7 µm in diameter, formed primarily on the edges of the plateau, with a few droplets on the top surface. This can be compared to the SEM image in Fig. 4(c) where the larger cavity-like features have about the same dimensions. Therefore, we can directly observe the formation of micro-droplets at the cavities generated by the chemical etch process.

This is further established by shining UV light on the structure and observation of the fluorescence of the Rhodamine B dye. The Fig. 5b shows that fluorescence from the dye is clearly visible from the top plateau of the microneedle, that is from the droplets as observed in the visible light microscopy. No fluorescence was observed from the walls of the microneedle, indicating that smooth facets do not store any liquid. We can therefore conclude that with proper choice of needle geometry and etch process, fluid can be selectively stored at the top of the microneedle, thereby reducing consumption of expensive or dangerous drugs during the injection process.

4. Conclusions

In this paper a low cost hybrid etching technique employing both isotropic and anisotropic etch chemistries was developed to generate well defined microneedles with small flat top which may include specific micro cavities for fluid storage. While the formation of smooth facets by wet chemical etch using KOH has been widely understood, this technique alone is not adequate for routine generation of sharp needles, as any over-etch can lead to rounding of the tips, and under-

etch will lead to large top plateaus. We have developed a novel technique incorporating thermal oxidation, oxide etch and subsequent isotropic etch of silicon, that can reduce the top plateau size to as low as 10 μm for needles 100 μm in height without a significant loss of mechanical rigidity. These microneedle arrays are compatible with surface scrape processes of drug delivery. Under optimized conditions, these process steps can be employed to generate micro-cavities surrounding the tip of the microneedle, generated by local variations in the oxidation and etch rates, which can be useful in transdermal drug delivery. The estimated volume of the microcavities can range from 0.02 nl to 0.06 nl per needles, and for a 100 × 100 needle array, the total volume is estimated to be approximately 600 nl.

Acknowledgements

Alakananda Das (09/028 (0946)/2015-EMR-I) would like to acknowledge the Council of Scientific and Industrial Research (CSIR) Senior Research Fellowship scheme and Chirantan Singha would like to acknowledge the Department of Science and Technology (DST) INSPIRE fellowship (IF120257) for funding their respective work. We are also grateful to Sayantani Sen, Pallabi Pramanik, Arpita Das, Pushan Guha Roy and Suchismita Paul for their invaluable help and advice. The work has been funded partially by TEQIP Phase II and UPE-II program at the University of Calcutta.

References

[1] M.R. Prausnitz, R. Langer, Transdermal drug delivery, Nat. Biotechnol. 26 (2008) 1261–1268, https://doi.org/10.1038/nbt.1504.
[2] S. Henry, D.V. McAllister, M.G. Allen, M.R. Prausnitz, Microfabricated microneedles: a novel approach to transdermal drug delivery, J. Pharm. Sci. 87 (1998) 922–925, https://doi.org/10.1021/js980042+.
[3] J.H. Park, M.G. Allen, M.R. Prausnitz, Biodegradable polymer microneedles: fabrication, mechanics and transdermal drug delivery, J. Control. Release 104 (2005) 51–66, https://doi.org/10.1016/j.jconrel.2005.02.002.
[4] P.R. Miller, X. Xiao, I. Brener, D.B. Burckel, R. Narayan, R. Polsky, Microneedle-based transdermal sensor for on-chip potentiometric determination of K+, Adv. Healthc. Mater. 3 (2013) 876–881, https://doi.org/10.1002/adhm.201300541.
[5] P.V. Damme, F. Oosterhuis-Kafeja, M. Van der Wielen, Y. Almagor, O. Sharon, Y. Levin, Safety and efficacy of a novel microneedle device for dose sparing intradermal influenza vaccination in healthy adults, Vaccine 27 (2009) 454–459, https://doi.org/10.1016/j.vaccine.2008.10.077.
[6] M.R. Prausnitz, Microneedles for transdermal drug delivery, Adv. Drug Deliver. Rev. 56 (2004) 581–587, https://doi.org/10.1016/j.addr.2003.10.023.
[7] K. Van der Maaden, R. Luttge, P.J. Vos, J. Bouwstra, G. Kersten, I. Ploemen, Microneedle-based drug and vaccine delivery via nanoporous microneedle arrays, Drug Deliv. and Transl. Res. 5 (2015) 397–406, https://doi.org/10.1007/s13346-015-0238-y.
[8] M. Ochoa, C. Mousoulis, B. Ziaie, Polymeric microdevices for transdermal and subcutaneous drug delivery, Adv. Drug Deliver. Rev. 64 (2012) 1603–1616, https://doi.org/10.1016/j.addr.2012.09.035.
[9] J.W. Lee, J.H. Park, M.R. Prausnitz, Dissolving microneedles for transdermal drug delivery, Biomaterials 29 (2008) 2113–2124, https://doi.org/10.1016/j.biomaterials.2007.12.048.
[10] I.C. Lee, J. He, M. Tsai, K. Lin, Fabrication of a novel partially dissolving polymer microneedle patch for transdermal drug delivery, J. Mater. Chem. B 3 (2015) 276–285, https://doi.org/10.1039/c4tb01555j.
[11] W. Martanto, S.P. Davis, N.R. Holiday, J. Wang, H.S. Gill, M.R. Prausnitz, Transdermal delivery of insulin using microneedles in vivo, Pharm. Res. 21 (2004) 947–952, https://doi.org/10.1023/B:PHAM.0000029282.44140.2e.
[12] S. Hashmi, P. Ling, G. Hashmi, M. Reed, R. Gaugler, W. Trimmer, Genetic transformation of nematodes using arrays of micromechanical piercing structures, Biotechniques 19 (1995) 76670.
[13] D.V. McAllister, P.M. Wang, S.P. Davis, J.H. Park, P.J. Canatella, M.G. Allen, M.R. Prausnitz, Microfabricated needles for transdermal delivery of macromolecules and nanoparticles: fabrication methods and transport studies, P. Natl. Acad. Sci. Usa. 100 (2003) 13755–13760, https://doi.org/10.1073/pnas.2331316100.
[14] J. Ji, F.E.H. Tay, J. Miao, C. Iliescu, Microfabricated silicon microneedle Array for transdermal drug delivery, J. Phys. : Conference Series 34 (2006) 1127–1131, https://doi.org/10.1088/1742-6596/34/1/186.
[15] L.T. Canham, Bioactive silicon structure fabrication through nanoetching techniques, Adv. Mater. 7 (1995) 1033–1037, https://doi.org/10.1002/adma.19950071215.
[16] C. Jäger, B. Finkenberger, W. Jäger, M. Christophersen, J. Carstensen, H. Föll, Transmission electron microscopy investigations of the formation of macropores in n- and p-Si(001)/(111), Mater. Sci. Eng. (70) (2000) 199–204, https://doi.org/10.1016/s0921-5107(99)00264-0 B69.
[17] J. Salonen, A.M. Kaukonen, J. Hirvonen, V.P. Lehto, Mesoporous silicon in drug delivery applications, J. Pharm. Sci. 97 (2008) 632–653, https://doi.org/10.1002/jps.20999.
[18] S.P. Low, N.H. Voelcker, L.T. Canham, K.A. Williams, The biocompatibility of porous silicon in tissues of the eye, Biomaterials 30 (2009) 2873–2880, https://doi.org/10.1016/j.biomaterials.2009.02.008.
[19] A.A. Hamzah, N.A. Aziz, B.Y. Majlis, J. Yunas, C.F. Dee, B. Bais, Optimization of HNA etching parameters to produce high aspect ratio solid silicon microneedles, J. Micromech. Microeng. 22 (2012) 095017–0905027, https://doi.org/10.1088/0960-1317/22/9/095017.
[20] S.V. Kalinin, A.V. Egorkin, Two-dimensional thermal oxidation of nonplanar silicon surfaces, Russ. Microelectron. 44 (2015) 114–126, https://doi.org/10.1134/S1063739714060055.